Supporting Information

Authors and Affiliations

Yilong Chang[1], Qi Li[1], Shuai Wu[1], Benjamin Pulli[2], Darren Samli[3], Paul Yock[4], Jeremy J. Heit[2], Ruike Renee Zhao[1]

[1]Department of Mechanical Engineering, Stanford University School of Engineering, Stanford, CA 94305, USA.

[2]Department of Radiology, Stanford University School of Medicine, Stanford, CA 94305, USA.

[3]Department of Pathology, Stanford University School of Medicine, Stanford, CA 94305, USA.

[4]Department of Bioengineering, Stanford University School of Engineering, Stanford, CA 94305, USA.

Corresponding author

Correspondence to: Ruike Renee Zhao (rrzhao@stanford.edu)

Supplementary Note 1 | Experimental procedure of milli-spinner capturing object under flow

Plastic balls with varied diameters (1.5, 2, and 2.5 mm) are 3D printed using Form 3+ (Formlabs, USA) printer with Formlabs Grey resin. A ball is placed in front of a milli-spinner (OD = 2.5 mm) inside a silicone tube with an inner diameter of 3 mm filled with water as shown in **Extended Data Fig. 2f**. The milli-spinner is activated to spin under a predetermined frequency drawing the ball to its front surface. A controlled water flow is initiated from the inlet and gradually increases. The resisted flow speed in **Extended Data Fig. 2g** and **2h** is referred as the fluid speed when the milli-spinner fails to capture the ball.

Supplementary Note 2 | Computational fluid dynamics (CFD) simulations on suction and shear performance of different milli-spinner designs

In this study, the selection of milli-spinner design for clot-debulking considers two aspects: suction and shear. CFD analyses are conducted to quantitatively assess the suction abilities of four different designs (see **Supplementary Fig. 2a**) inside a tube with a diameter D_{tube} of 3 mm. The centerline pressure drop along the axial direction of a milli-spinner reveals differences between the hollow cylinder and the hollow cylinder with slit design. The findings indicate that the slit not only enhances suction performance but also shifts the location of maximum pressure drop to the inside of the milli-spinner cavity (**Supplementary Fig. 2b**). This structure modification enhances the milli-spinner object capture ability, as shown in **Extended Data Fig. 2b**. In addition, adding fin features strengthens suction performance, shown by a maximum centerline pressure drop of 8.39 kPa. The comparison of pressure contour plots of varied planes perpendicular to the milli-spinner axial direction (**Supplementary Fig. 2c)** clearly demonstrates the superior suction capabilities of fin and slit design and, consequently, the clot compression capability.

We further investigate the distribution of shear forces generated by different milli-spinner designs. We compute the generated shear force across successive cross-sections along the axial direction (**Supplementary Fig. 2d)**. The milli-spinner with fin and slit design is shown to produce the highest shear force of 2.25 mN at the milli-spinner front plane in all four milli-spinner designs. Additionally, it exhibits the lowest decay of shear force along the axial direction compared to the other designs. The shear stress contours of the four milli-spinner designs at the milli-spinner front plane are shown in **Supplementary Fig. 2d**. The fin and slit design exhibits the highest shear stress distribution at the milli-spinner front surface.

Supplementary Note 3 | CFD simulations on suction and shear performance comparison of different milli-spinner designs with less boundary effect

Additional CFD simulations comparing the suction and shear ability of milli-spinner designs (**Supplementary Fig. 3a**) with D_{tube} of 10 mm are provided. From the flow velocity contour with streamline (**Supplementary Fig. 3b**), it is evident that the addition of slit feature has increased high flow velocity

gradient by allowing flow to be sucked through the milli-spinner surface front hole and escape out from slits. The milli-spinner with fin and slit exhibits the highest centerline pressure drop (**Supplementary Fig. 3c**). Additionally, the shear stress generated at the milli-spinner front surface plane is also highest for the fin and slit design and remains to be the highest along the axial direction among different designs. (**Supplementary Fig. 3d**).

Supplementary Note 4 | Experimental setup and procedure of clot-debulking in a straight tube

The setup is constructed as a three-way channel that allows water inlet and outlet and milli-spinner insertion (**Supplementary Fig. 4**). The outlet is connected to a 3 mm inner diameter silicone tube while the inlet is connected to a homemade pulsatile flow source. The pump provides 60 beats per minute pulsatile flow with an average flow speed of 1.02 $cm \cdot s^{-1}$. The milli-spinner is inserted into the three-way channel from the back end, center-aligned with the 3 mm silicon tube. A clot is cut into a predetermined length and also weighted to ensure size consistency across experiments. The clot is introduced from the outlet of the tube and placed in front of the milli-spinner blocking the entire lumen. Subsequently, the milli-spinner is set to spin at a predetermined frequency driven by the motor and draws the clot to its front tip. Once the clot is in contact with the milli-spinner, the pulsatile flow pump is activated.

Supplementary Note 5 | Clot volume reduction measurement during the clot-debulking process

The RGB images of the clot are extracted from the clot-debulking video at a 2 s interval and are converted to binary images using MATLAB with a threshold value of 0.18. The RGB images and binary images demonstrating the clot volume reduction process are shown in **Supplementary Fig. 5**. The rotating clot is assumed to be axisymmetric and the black pixels in the binary image are revolved into 3D to obtain the clot volume.

Supplementary Note 6 | Experimental setup and procedure of *in-vitro* clot-debulking in pulmonary artery flow model

The *in-vitro* pulmonary artery flow model setup comprises several components shown in **Supplementary Fig. 8**, including a motor, a flexible shaft (Torque rope 1×7, ASAHI INTECC CO., LTD, Japan), a sleeve, a milli-spinner with OD = 2.5 mm, an 8-French shuttle sheath (Flexor shuttle, Cook Medical, USA), 60 ml syringe, the homemade pulsatile flow pump, and a pulmonary flow model. The flexible shaft, connected to the motor, is inserted through the sleeve (5-French angiographic catheter, Cordis Corporation, USA) and the milli-spinner is glue fixed on the flexible shaft's distal end. The 8-French shuttle sheath is inserted into the pulmonary flow model reaching the clot proximal end. Subsequently, the flexible shaft and sleeve are inserted through the sheath reaching its distal end. The syringe pump draws water from the reservoir and

provides 60 bpm water flow through the inlet of the model with an average flow speed of 0.14 $cm \cdot s^{-1}$. The milli-spinner is activated, with the spinning frequency set to 10k rpm. To ensure firm compression between the clot and the milli-spinner, manual aspiration is performed using a 60 ml syringe, capable of generating a vacuum pressure of -29 inHg[1].

Supplementary Note 7 | Experimental setup and procedure of *in-vitro* clot-debulking in cerebral artery flow model

The *in-vitro* cerebral artery flow model setup includes a Neuro Max (Penumbra, Inc.), a 6-French aspiration catheter, a flexible shaft, and a sleeve. A milli-spinner with a diameter of 1.2 mm is utilized to fit through the catheter lumen. After a clot is introduced, the 6-French aspiration catheter is navigated through Neuro Max to the middle cerebral artery section of the cerebral artery flow model (Dewei Medical Technology Co., Ltd, China) reaching the clot proximal end. The Milli-spinner system is then inserted through the aspiration catheter reaching the catheter distal end. The milli-spinner is activated, with a spinning frequency of 6k rpm aided by vacuum aspiration generated by a pump (Gomco Pump, Allied Healthcare Products, Inc.) to ensure firm compression of the clot onto the front surface of the milli-spinner.

Supplementary Note 8 | Experimental setup and procedure of *in-vivo* clot-debulking in swine model

All procedures are conducted in accordance with international guidelines and are approved by our institutional review board.

In the demonstration depicted in **Fig. 5c-d**, a swine weighing 55 kg is utilized as the experimental model. Following the anesthesia of the swine, an 8-French, 11cm vascular sheath (Cordis Corporation, USA) is placed in the right femoral artery. Next, a 6-French shuttle sheath (Flexor shuttle, Cook Medical, USA) is introduced over a 5-French, 125 cm diagnostic catheter (VER, Cordis Corporation, USA) over an 0.035 inch angled guidewire. The construct is navigated into the renal artery using continuous fluoroscopic guidance, and the diagnostic catheter and guidewire are removed. Digitally subtracted angiography (DSA) using iodinated contrast (Isovue, Bracco Diagnostics, Italy) is performed to demonstrate the catheter position and the arterial anatomy of the kidney. Next, a clot (30% RBC content) is injected through the shuttle sheath into the renal artery. DSA is again performed to characterize the arterial occlusion due to the injected clot, and these images are used as roadmap angiography guidance for subsequent MT the milli-spinner device, which is introduced through the 6-French shuttle sheath. Milli-spinner motion is initiated and maintained for 2 minutes with concomitant vacuum aspiration at -27 inHg, which is generated by the pump directly into the aspiration catheter or milli-spinner device. After 2 minutes, the milli-spinner is withdrawn from the swine model while maintaining continuous aspiration. Additional back-bleeding from the 6-French shuttle sheath is performed to ensure that any clot fragments that are dislodged into the shuttle

sheath by the MT procedure are removed. DSA is again performed through the shuttle sheath to assess the degree of revascularization that is achieved.

In the demonstration shown in **Fig. 5g-i**, a swine with a weight of 64 kg is used. After the anesthesia of the swine, the vascular sheath is placed in the right common carotid artery. A Neuro Max sheath is introduced to facial arteries in the same manner described above. A 30% RBC content clot is introduced through Neuron Max to induce vessel occlusion in facial arteries. A Vecta 74 (Stryker Corporation, USA) catheter is advanced through the Neuron Max over the guidewire to clot occlusion location. After removing the guidewire, the milli-spinner is inserted through the Vecta 74 catheter reaching the clot proximal end. The spinning motion is then initiated and maintained for 2 minutes with -27 inHg vacuum aspiration engaged onto Vecta 74. Then, the milli-spinner and Vecta 74 catheter are withdrawn together from the swine model while aspiration and spinning are kept on. After milli-spinner thrombectomy, DSA is performed through the Neuron Max to evaluate the success of the MT procedure.

In the demonstration depicted in **Extended Data Fig. 6**, a swine weighing 66 kg is utilized. An 8-French vascular sheath is placed in the right femoral artery and vessel occlusion in renal arteries is induced by injecting a clot (30% RBC content) through Neuro Max. The milli-spinner thrombectomy is performed with Vecta 74 catheter following the procedure described above. After milli-spinner thrombectomy, DSA is performed through the Neuron Max to evaluate the success of the MT procedure.

In the demonstration depicted in **Extended Data Fig. 7**, a swine weighing 70.4 kg is utilized. An 8-French vascular sheath is placed in the right common carotid artery. Vessel occlusion and the milli-spinner thrombectomy are conducted following the procedure described above. A Vecta 74 catheter is utilized. After milli-spinner thrombectomy, DSA is performed through the Neuron Max to evaluate the success of the MT procedure.

In the demonstration depicted in **Extended Data Fig. 8**, a swine weighing 70.4 kg is utilized. An 8-French vascular sheath is placed in the right common carotid artery. Vessel occlusion is inducted following the procedure described above. Direct aspiration thrombectomy is first performed using a 6-French aspiration catheter. The catheter is advanced to the clot proximal end, and vacuum aspiration of -27 inHg is applied to the catheter. After 2 minutes, the aspiration catheter is pulled out of the swine, and vacuum aspiration is turned off. Subsequently, back-bleeding from the Neuro Max is performed to ensure no clot fragment residual inside the sheath. DSA is performed through the Neuron Max to evaluate the success of the MT procedure. After realizing failed direct aspiration thrombectomy, a 6-French aspiration catheter is reintroduced and milli-spinner thrombectomy is performed following the procedures described above. After milli-spinner thrombectomy, DSA is performed through the Neuron Max to evaluate the success of the MT procedure.

Supplementary Note 9 | Direct aspiration thrombectomy in swine model

In the demonstration depicted in **Extended Data Fig. 5**, a swine weighing 55 kg is used, and the care of the animal and vascular access are done as noted above. Next, a 6-French shuttle sheath is advanced to the proximal end of the clot. Vacuum aspiration by pump is applied to the shuttle sheath, which generates a constant -27 inHg vacuum pressure against the clot for 2 minutes. Subsequently, back-bleeding from the 6-French shuttle sheath is performed. DSA is performed through the shuttle sheath to evaluate the success of the MT procedure.

Supplementary Note 10 | CFD simulations

CFD simulations are conducted in COMSOL Multiphysics 6.1 (COMSOL Inc., USA) for the investigation of the flow field. The spinning motion of milli-spinners is modeled at different spinning frequencies, ranging from 10k to 40k rpm. The corresponding Reynolds number (Re) ranges from 3273 to 13090. The k-ε turbulence model is implemented to solve the Navier-Stokes (N-S) momentum equation for Newtonian incompressible flow. The frozen rotor method is implemented, where the motion is modeled by incorporating the Coriolis and centrifugal forces into the N-S momentum equation. This means that the milli-spinner does not physically rotate during the simulation; instead, the effects of rotation and associated momentum terms are imparted to the flow. The model incorporates one stationary and one rotating domain with subtracted milli-spinner geometry, with the interface acting as a moving reference frame. The rotating domain exhibits an angular velocity component near the wall boundary. Boundary conditions are defined as follows: zero velocity at the inlet to the milli-spinner base, zero pressure at the outlet, a no-slip condition at the milli-spinner surfaces, and the fixed outer pipe walls. The simulation, in comparison to micro-PIV results, is conducted in a sealed tank, where all the surfaces are treated as fixed walls. In **Fig. 2**, **Supplementary Fig. 2** and **3**, shear force is calculated by integrating the shear stress across a particular surface. This calculation is repeated across successive cross-sections along the milli-spinner axial direction to map out the distribution of shear forces away from the milli-spinner front surface.

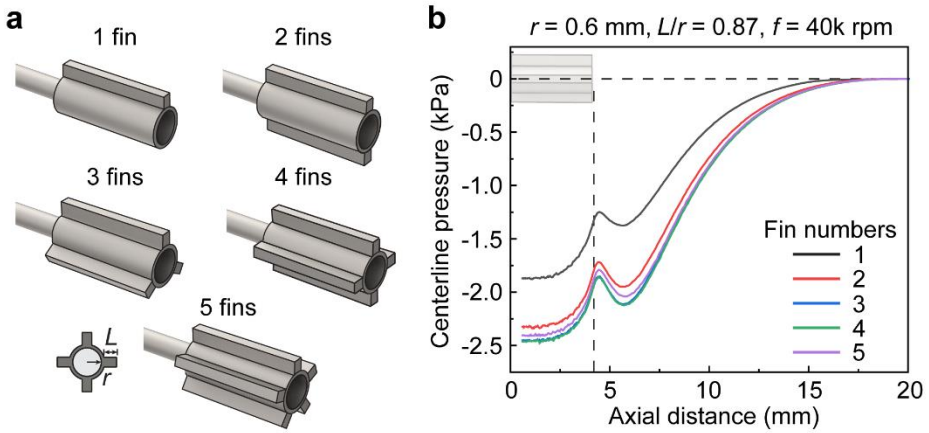

Supplementary Fig. 1 | CFD simulations on suction comparison of milli-spinner with varied fin numbers. a, Milli-spinner with fin design schematics showing fin layout of designs with 1, 2, 3, 4, and 5 fins. **b**, Centerline pressure distribution with respect to the axial distance of the milli-spinner designs in (a) at f = 40k rpm with tube diameter D_{tube} = 3 mm.

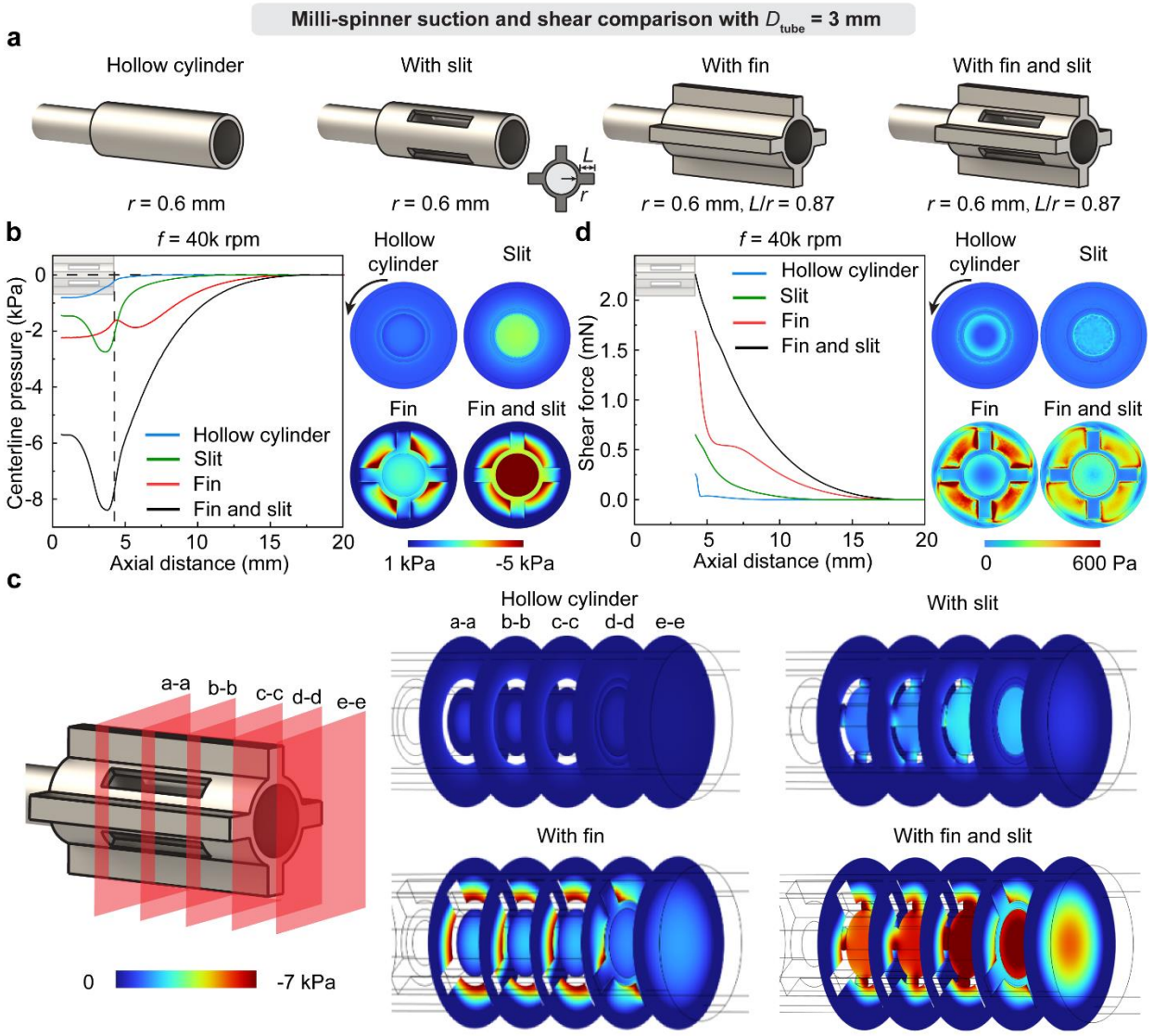

Supplementary Fig. 2 | CFD simulations on milli-spinner geometric optimization for enhanced suction and shear. a, Different milli-spinner designs (r = 0.6 mm, normalized fin length L/r = 0.87): hollow cylinder, hollow cylinder with slit, hollow cylinder with fin, and hollow cylinder with fin and slit. **b**, Centerline pressure distribution with respect to the axial distance of the milli-spinner designs in (a) at f = 40k rpm with D_{tube} = 3 mm. Pressure contour at the front surface plane of the milli-spinner designs in (a) at f = 40k rpm. **c**, Pressure contour at different planes perpendicular to axial direction of milli-spinners in (a) at f = 40k rpm. From left to right, the planes are plane a-a located at the beginning of the slit, plane b-b located at the mid of the slit, plane c-c located at the end of the slit, plane d-d located at the milli-spinner front surface, and plane e-e located in front of the milli-spinner. Each plane is placed 1.05 mm apart. **d**, Shear force with respect to the axial distance of the milli-spinner designs in (a) at f = 40k rpm. Shear stress contour at the front surface plane of the milli-spinner designs in (a) at f = 40k rpm.

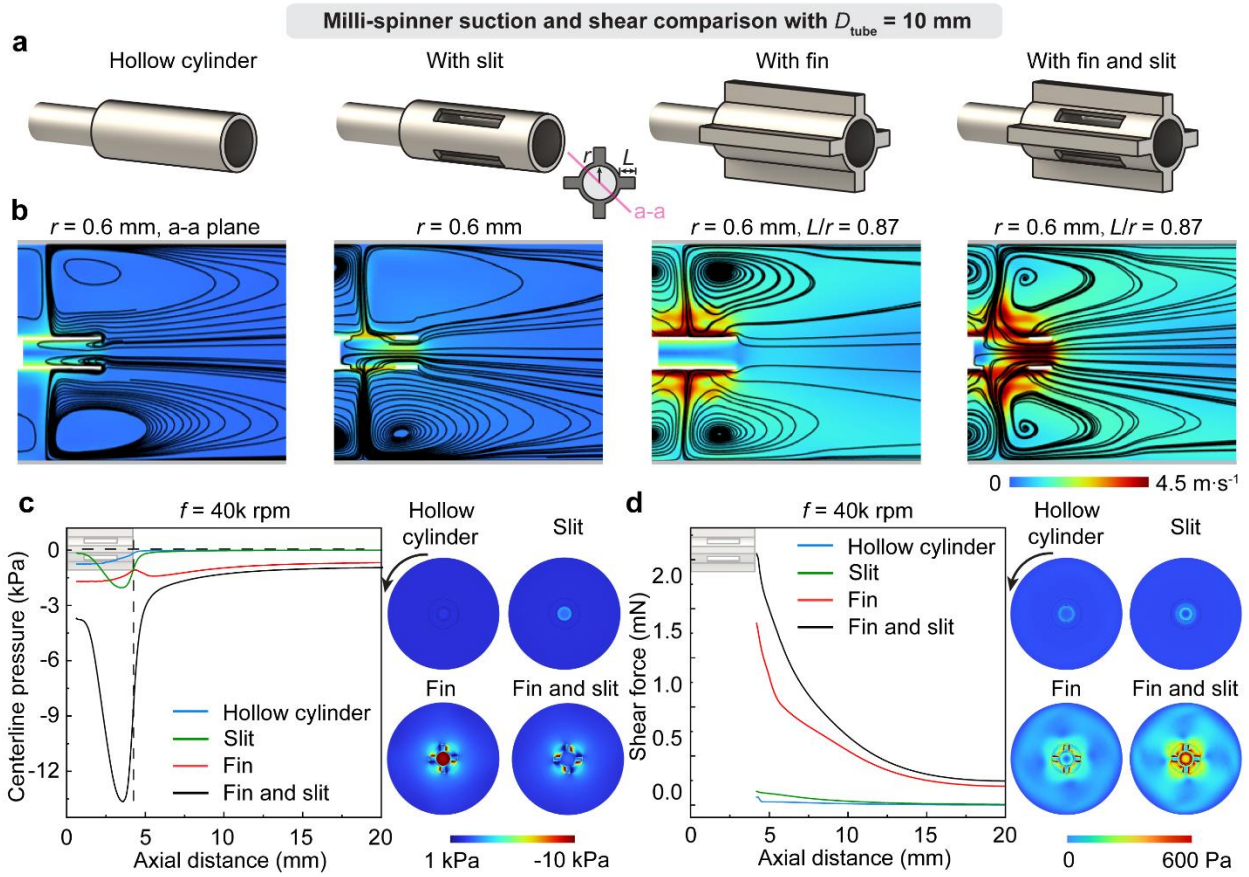

Supplementary Fig. 3 | CFD simulations on milli-spinner for suction and shear with less boundary effect. a, Different milli-spinner designs (r = 0.6 mm, normalized fin length L/r = 0.87): hollow cylinder, hollow cylinder with slit, hollow cylinder with fin, and hollow cylinder with fin and slit. **b**, Corresponding velocity contour with streamlines of the milli-spinner designs in (a) illustrate flow towards the milli-spinner's cavity at f = 40k rpm with D_{tube} = 10 mm. **c**, Centerline pressure distribution with respect to the axial distance of the milli-spinner designs in (a) at f = 40k rpm. Pressure contour at the front surface plane of the milli-spinner designs in (a) at f = 40k rpm. **d**, Shear force with respect to the axial distance of the milli-spinner designs in (a) at f = 40k rpm. Shear stress contour at the front surface plane of the milli-spinner designs in (a) at f = 40k rpm.

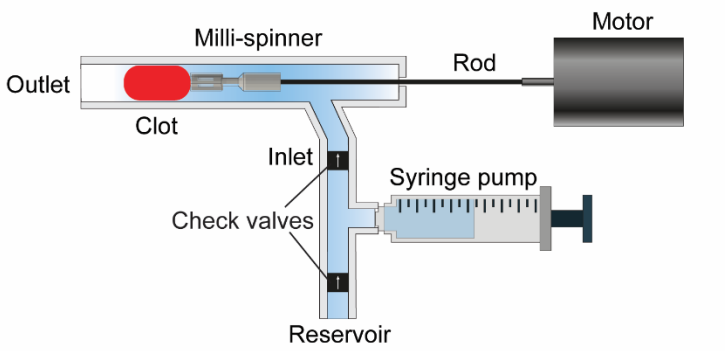

Supplementary Fig. 4 | Schematic of experimental setup for clot-debulking in the straight tube.

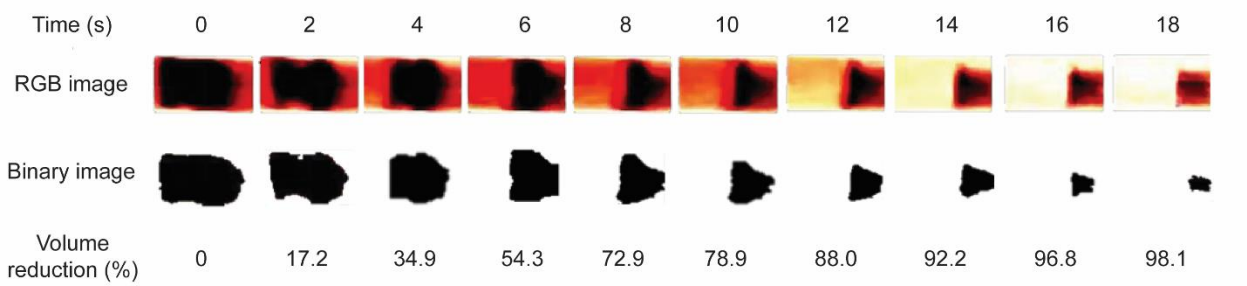

Supplementary Fig. 5 | RGB and binary images of a clot during the clot-debulking process. The clot-debulking test is conducted using a 2.5 mm OD milli-spinner debulking a 6.5 mm long whole blood formed clot at f = 40k rpm with D_{tube} = 3 mm.

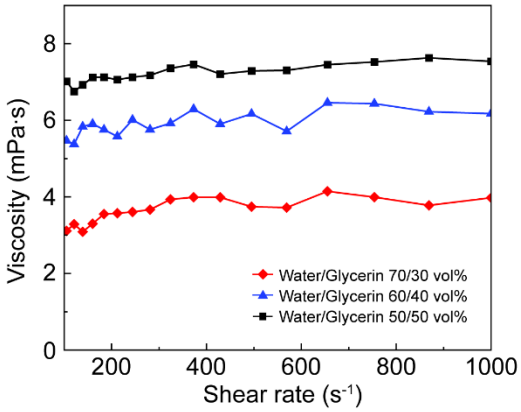

Supplementary Fig. 6 | Viscosity measurement of water and glycerin mixture. The reported viscosity in the main text is the viscosity measured under shear rate of 100 s^{-1}.

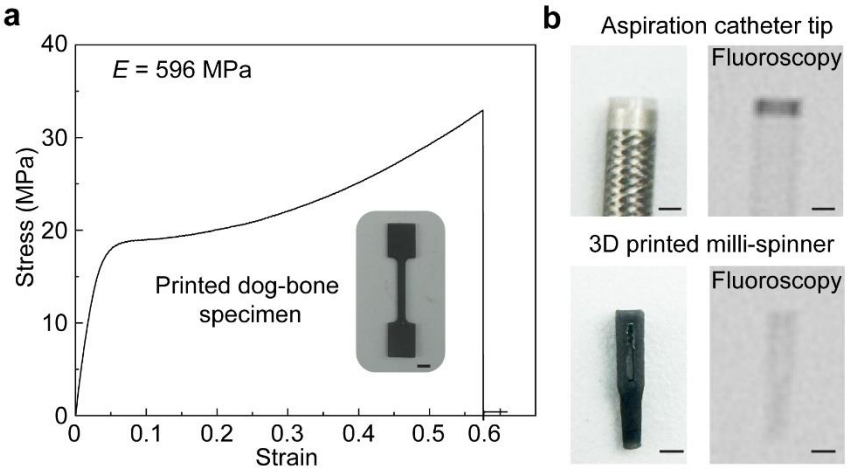

Supplementary Fig. 7 | Radio-opaque milli-spinner material characterization. a, Stress-strain curve of a 3D printed radio-opaque dog-bone specimen. Young's modulus of the material is determined by taking the slope corresponding to 1% strain on the stress-strain curve. Scale bar: 2 mm. **b**, Radio-opacity comparison between the aspiration catheter tip and the printed radio-opaque milli-spinner (OD = 1.2 mm). Scale bars: 1 mm.

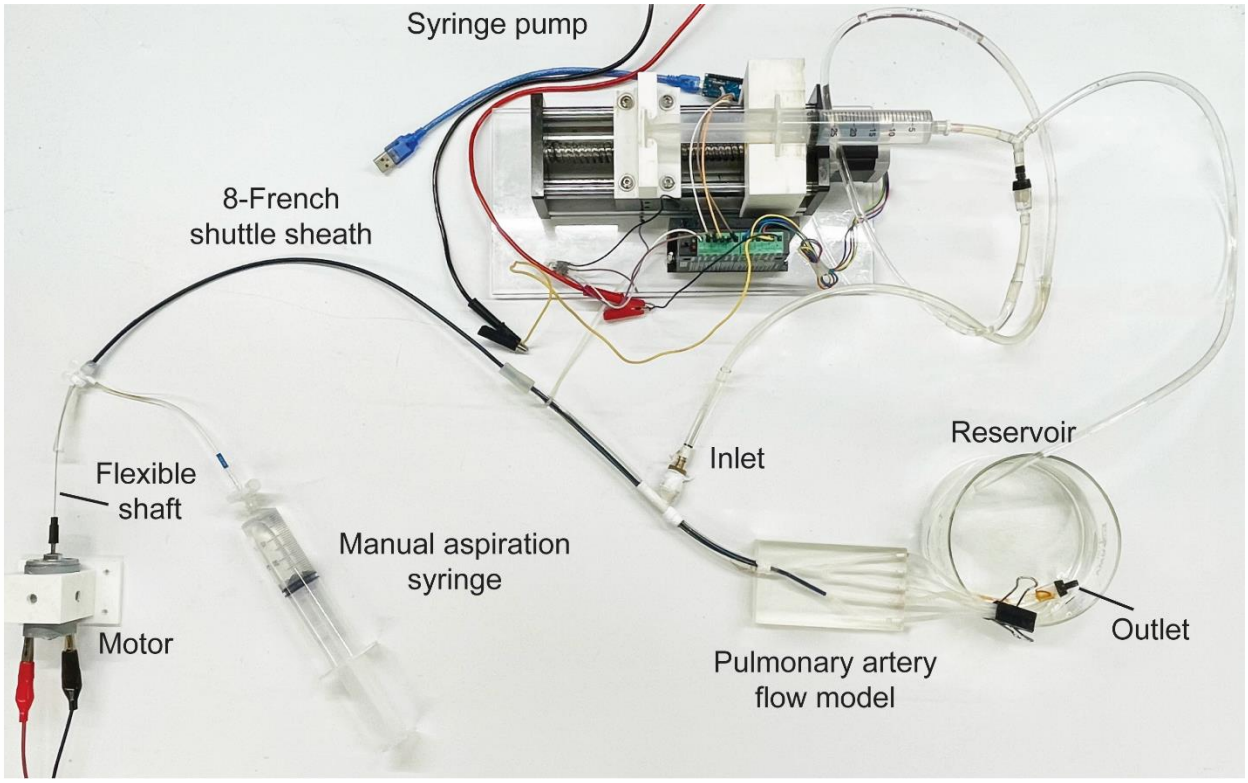

Supplementary Fig. 8 | Experimental setup of *in-vitro* clot-debulking in pulmonary artery flow model.

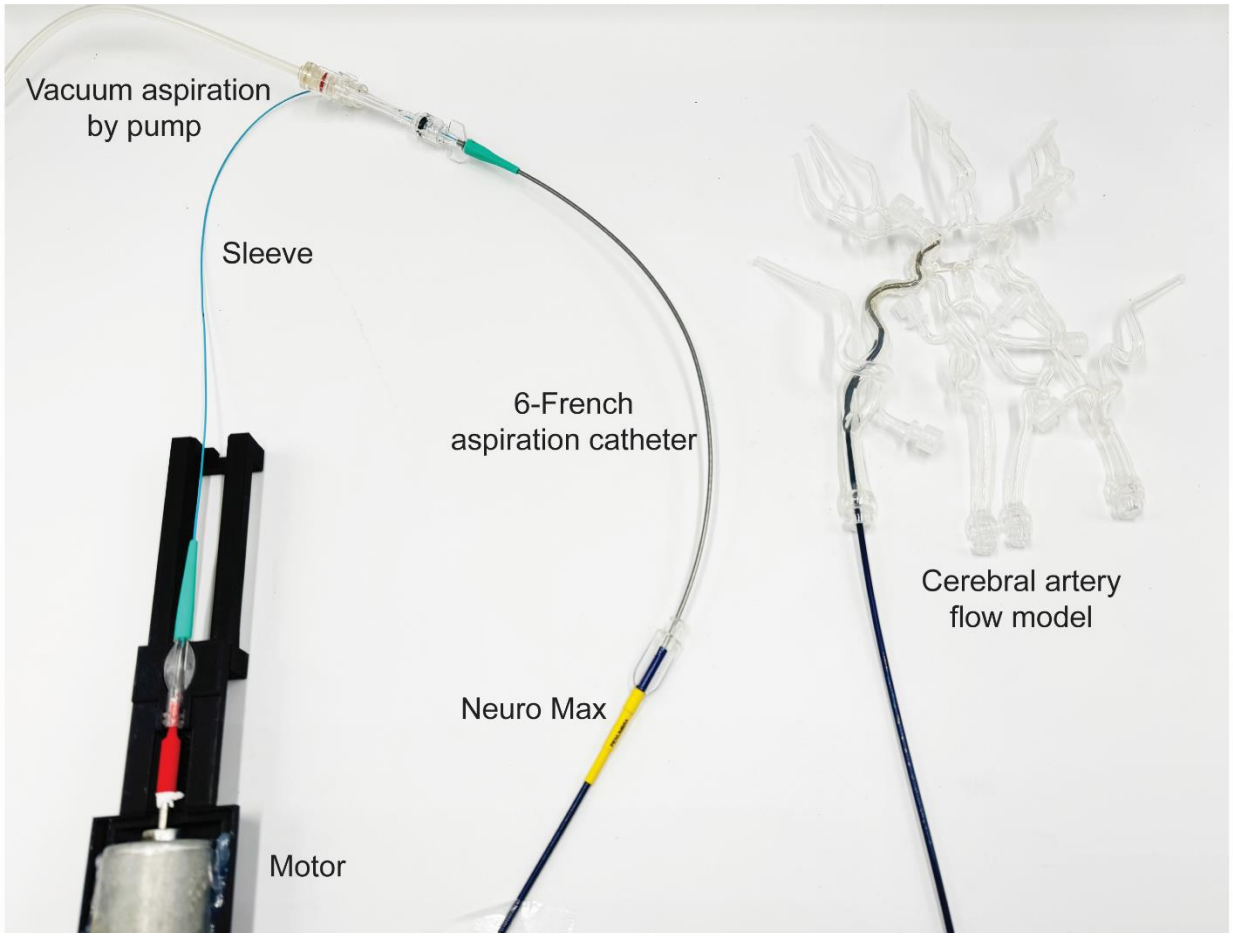

Supplementary Fig. 9 | Experimental setup of *in-vitro* clot-debulking in cerebral artery flow model.

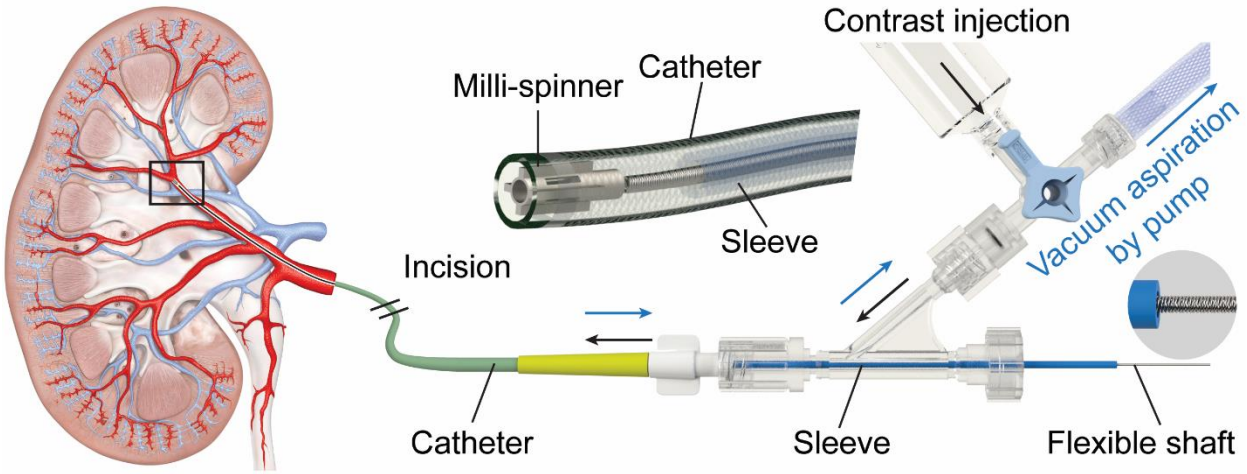

Supplementary Fig. 10 | Schematic of experimental setup of *in-vivo* clot-debulking in swine model. The schematic shows the milli-spinner setup utilized in the clot-debulking test in the swine renal arteries. The same system is used for the clot-debulking test in the swine facial arteries.

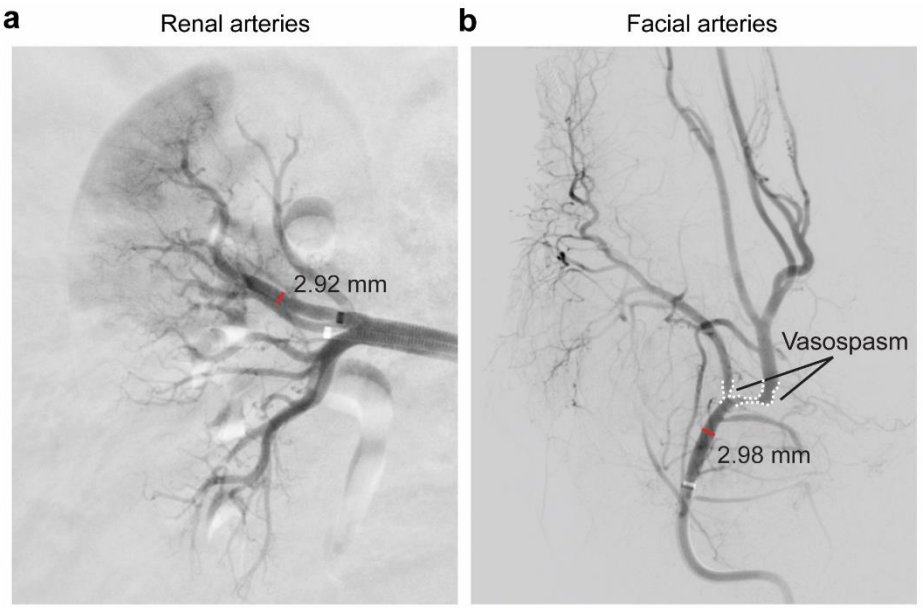

Supplementary Fig. 11 | Swine renal and facial arteries size measurement. a, Swine renal arteries size measurement showing a vessel diameter of around 3 mm at the clot-debulking location. **b**, Swine facial arteries size measurement showing a vessel diameter of around 3 mm at the clot-debulking location. The measurement is done using Horos open-source medical image viewer.

1 Kim, S. & Lee, J. Y. Comparison of vacuum pressures and suction forces generated by different pump systems for aspiration thrombectomy. *Frontiers in Neurology* **13**, 978584 (2022).